

Cobalt Substitution in CuFe_2O_4 spinel and its influence on the crystal structure and phonons

M. D. P. Silva,[†] F. C. Silva,[†] F. S. M. Sinfrônio,[†] Alexandre Rocha Paschoal,[‡] E. N. Silva,[†] and Carlos William de Araujo Paschoal^{*,¶,||}

Universidade Federal do Maranhão, Universidade Federal do Ceará, Departamento de Física, CCET, Universidade Federal do Maranhão, 65085-580, São Luís - MA, Brazil, and Department of Materials Science and Engineering, University of California Berkeley, 94720-1760, Berkeley - CA, United States

E-mail: paschoal.william@gmail.com

Abstract

In this work nanometric spinel $\text{Co}_{1-x}\text{Cu}_x\text{Fe}_2\text{O}_4$ powders were obtained by polymeric precursors method at several annealing temperatures between 700 and 1200 °C. The samples were characterized by means of X-ray powder diffraction, confirming the ideal inverse spinel structure for CoFe_2O_4 sample and the tetragonal distorted inverse spinel structure for CuFe_2O_4 sample. Based on FWHM evaluation, we estimated that crystallite sizes varies between 27 and 37 nm for the non-substituted samples. The optical-active modes were determined by infrared and Raman spectroscopies. The phonon spectra showed a local tetragonal distortion for mixed samples.

*To whom correspondence should be addressed

[†]Departamento de Química, CCET, Universidade Federal do Maranhão, 65085-580, São Luís-MA, Brazil

[‡]Departamento de Física, Universidade Federal do Ceará, Campus do Pici, 60455-760, Fortaleza - CE, Brazil

[¶]Departamento de Física, CCET, Universidade Federal do Maranhão, 65085-580, São Luís - MA, Brazil

[§]Department of Materials Science and Engineering, University of California Berkeley, 94720-1760, Berkeley - CA, United States

^{||}Author whose correspondence should be addressed: Phone +55 98 3301.9209; Fax: +55 98 3301 8204

Keywords: Spinel, CoFe_2O_4 , CuFe_2O_4 , Raman, Infrared, X-ray powder diffraction

Introduction

Multiferroics are singular materials that exhibit simultaneously two ferroic orders, usually electric and magnetic, with a magnetoelectric coupling between them in some cases. These materials have attracted much attention due to their potential technological applications. As such, multiferroic compounds bring new functionalities to spintronics and new device possibilities, such as memories, sensors, actuators and tunable filters.¹⁻⁵ The most investigated multiferroic compound is the perovskite BiFeO_3 .⁶⁻¹⁴ However, the long search for the control of electrical properties by magnetic fields has been recently led to in a group of materials known as "frustrated magnets", such as: the perovskites REMnO_3 ¹⁵⁻¹⁷ and REMn_2O_5 ¹⁸⁻²¹ (with RE being rare earth ions), in the spinels CuFeO_2 ^{22,23} and CoCr_2O_4 ,²⁴ and the Y-type hexagonal ferrites $(\text{Ba, Sr})_2\text{Zn}_2\text{Fe}_{12}\text{O}_{22}$,²⁵ among others.

The restricted number of pure multiferroic compounds is a consequence of the atomic arrangement specificity, since, theoretically, only 13 point groups can lead to the multiferroic behavior. In addition, by definition, ferroelectrics are insulators (3d transition metal oxides typically have ions which have an electronic distribution d^0), while ferromagnets need conduction electrons. The difficulties associated with the combination of electric and magnetic responses in a single phase compound can be solved by making two-phase multiferroic composites consisting of a ferroelectric component (e.g. $\text{PbZr}_{1-x}\text{Ti}_x\text{O}_3$ - PZT) and a ferromagnetic component (e.g. CoFe_2O_4).²⁶⁻³⁸ In such composites, the magnetoelectric effect is due to the interaction between elastic components of ferroelectric and ferromagnetic constituents. In such case, an electric field induces a voltage in the ferroelectric which is transferred to the ferromagnet, that causes the magnetization of the material. Since the magnetoelectric effect is higher if the coupling at the interface is higher, compounds with large surface areas (as in multilayer thin films and nanometric powders) and strongly ferroelastic are particularly interesting. This approach opens new routes to get a magnetoelectric response with

the specific choice, relationship and microstructure of the constituents. In fact, the magnetoelectric coefficients at room temperature which was achieved exceed those found in low-temperature single phase samples in three to five orders of magnitude. Thus, magnetoelectric multiferroic composites are on the boundary of the technological applications.^{3,4,39,40} So, as the spinels have been continuously employed to obtain good multiferroic composites, a careful attention has been given in last years to the synthesis of spinels in last years for different methods.⁴¹⁻⁶¹

Besides their extensively investigated ferromagnetic properties, Li-based spinels has been extensively investigated to be applied as electrode in batteries.^{???} Also, binary spinel ferrites like CdFe_2O_4 , NiFe_2O_4 , ZnFe_2O_4 and CuFe_2O_4 also show significant gas-sensing activity.⁶² Moreover, CuFe_2O_4 shows high electronic conductivity, high thermal stability and high activity as green anode for aluminum electrolysis.⁶³ Another important binary spinel-type ferrite is the cobalt ferrite CoFe_2O_4 due to its high cubic magnetocrystalline anisotropy, high coercivity, and moderate saturation magnetization, being such properties severely affected by to the concentration of divalent metal cation.^{59???}

Usually CoFe_2O_4 crystallizes in a spinel structure. The cationic distribution in the spinel structure can be described by the chemical formula $(\text{Fe}_{1-x}\text{Co}_x) [\text{Fe}_{1+x}\text{Co}_{1-x}]\text{O}_4$, where () and [] denote the tetrahedral *A* and octahedral *B* sites, respectively. The inversion parameter *x* is equal to 0 for inverse spinels and to 1, when the spinel is normal. CoFe_2O_4 spinel structure is predominantly inverse ($x = 0$), with Co^{2+} ions occupying mainly *B* sites while Fe^{3+} ions are distributed almost equally on *A* and *B* sites. The inversion index $(1 - x)$ depends on the thermal history of the sample.⁶⁴ By the other side, CuFe_2O_4 has a tetragonally deformed spinel structure, that is stretched along the $\langle 011 \rangle$ direction.⁶⁵ Yokoyama *et al.*⁶⁶ observed changes in the crystal structure of nanosized CuFe_2O_4 powders obtained by coprecipitation followed by annealing. They observed that the copper spinel is cubic at temperatures below 300 °C and tetrahedral over 400 °C. The formation of considerable quantities of Cu^+ in the lattice is the mechanism responsible for the transition from tetragonal to cubic structure.⁶⁶ As showed by Kester *et al.*,⁶⁷ through reduction reaction of quenched samples of CuFe_2O_4 , the formation of Cu^+ takes place, but its fraction in

the B-sublattice strongly depends on the synthesis procedures and on the subsequent temperature treatment. Nanosized particles of CuFe_2O_4 , obtained by a classical ceramic technology, have also been studied.⁶⁸ High temperature treatments lead to structural and magnetic surface disorders, which can be induced by the dispersion of different copper ions in the sublattices, by the arising of cations and oxygen vacancies, by the structure amorphisation, among others. Also, when the spinel is synthesized using classical solid state route with accurate stoichiometry ($x = 1$), it has a tetragonal structure.⁶⁹

However, independently of the cation present in the lattice, the physicochemical properties of such spinel-type ferrites depend on their microstructural properties, which are related, in turn, to the preparation methods of these compounds. Thus, several routes were used to produce these binary oxides such as hydrolysis,⁷⁰ ball-milling, solid state reaction, co-precipitation and sol gel methods, combustion processing etc.⁷¹ Since the synthesis route is crucial over the spectroscopic and structural properties of the spinel-type ferrites, the aim of this work was to evaluate the effect of cobalt isovalent substitution in CuFe_2O_4 spinels nanoparticles obtained by polymeric precursors method.

Materials and Methods

All samples were synthesized using the Polymeric Precursor Method, as follow: ferric chloride hexahydrate ($\text{FeCl}_3 \cdot 6\text{H}_2\text{O}$, Isofar), copper sulphate pentahydrate ($\text{CuSO}_4 \cdot 5\text{H}_2\text{O}$, Isofar) and cobalt chloride hexahydrate ($\text{CoCl}_2 \cdot 6\text{H}_2\text{O}$, Vetec) were used as purchased without further purification (pa purity). The precursor solutions of Fe, Cu and Co were prepared by adding the raw solids into an aqueous solution of citric acid ($\text{C}_6\text{H}_8\text{O}_7$, Nuclear), using stoichiometric quantities. Therefore, ethylene glycol ($\text{C}_2\text{H}_6\text{O}_2$, Nuclear) was added to the metallic solution, according to a molar ratio 1:3. This solution was heated at $110\text{ }^\circ\text{C}$ for 5 h in an oven to promote polymerization. Soon after, the polymerized gel was heated at $300\text{ }^\circ\text{C}$ for 1 h, under air atmosphere, to burn the organic matter and form a black solid mass (primary calcination). Such carbonaceous mass was grounded until

its particles were 100 Mesh sized and heat-treated at 300 °C for 12 hours (secondary calcination), under a high oxygen atmosphere, in order to produce oxygen vacancies in the solids. Finally, such precursor powders were annealed between 700–1200 °C (ternary calcination) in air for 4 h in Al₂O₃ crucibles, and the desired spinel compounds resulted.

Crystal structures of the annealed powders were examined using an X-ray diffractometer Xpert MPD (Panalytical), with Co K α radiation (40 kV and 40 mA), speed of 0.02° θ s⁻¹ and value ranging from 10 to 100 °. X-ray powder diffraction (XRD) patterns were compared with the Joint Committee Powder Diffraction Standards (JCPDS) data for the phase evaluation.

Crystallite sizes (D) of the samples were determined from X-ray line broadening analyzes, employing the Scherrer's equation:

$$D = \frac{K\lambda}{\beta \cos\theta} \quad (1)$$

where λ is the X-ray radiation wavelength ($\lambda = 1.78896 \text{ \AA}$), K is the Scherrer constant, β is the FWHM of the peak (in radians) and θ is the peak angular position.

The infrared spectra were obtained using an IR prestige-21 infrared spectrometer (Shimadzu), applying KBr as dispersant agent (1:100 wt./wt.) in the mid range: 400 up to 1000 cm⁻¹.

The confocal Raman spectra were acquired using an alpha 300 system microscope (Witec, Ulm, Germany), equipped with a highly linear (0.02%) stage, piezo-driven, and an objective lens from Nikon (20x, NA = 0.40). A Nd:YAG polarized laser ($\lambda = 532 \text{ nm}$) was focused with a diffraction-limited spot size ($0.61\lambda/\text{NA}$) and the Raman light was detected by a high sensitivity, back illuminated spectroscopic CCD behind a 600 g/mm grating. The final power at the end of the objective lens used to focus on the sample was 3 mW. The spectrometer used was an ultra-high throughput Witec UHTS 300 with up to 70% throughput, designed specifically for Raman microscopy. The integration time and number of accumulations were in average 60 s and 3, respectively.

Crystalline Structure and Group Theory

Both CoFe_2O_4 and CuFe_2O_4 crystallizes according to inverse spinel-based structure. Particularly, CuFe_2O_4 assumes a body centered tetragonal distorted inverse-spinel structure belonging to the space group $I4_1/amd(D_{4h}^{19})$, in which there are four molecules per unit cell ($Z = 4$). In this structure Fe/Cu, Fe and O atoms occupy 8d (C_{2h}), 4a (D_{2d}) and 16h (C_s) Wyckoff sites, respectively. On the other hand, CoFe_2O_4 shows a face centered cubic inverse-spinel structure, belonging to the space group $Fd\bar{3}m(O_h^7)$, with eight molecules per unit cell ($Z = 8$), in which Fe/Co, Fe and O atoms occupy 16d (D_{3d}), 8a (T_d) and 32e (C_{3v}) Wyckoff sites, respectively.

Since each structure contains 14 atoms in the primitive unit cell, there are 42 degrees of freedom and, consequently, 42 phonons are permitted for both structures. Using the Factor Group Analysis,⁷² the zone-center vibrational modes distribution was decomposed in terms of the irreducible representations for both O_h and D_{4h} factor groups (Table 1). Due to these site occupations, for both structures, Fe^B/M ($\text{M} = \text{Co}$ or Cu) atoms do not contribute to the Raman-active phonon spectra. Thus, any Raman assignments can be attributed to $(\text{Fe})^A$ and O ions, while the infrared spectra may be influenced by all constituent ions.

CuFe_2O_4 and CoFe_2O_4 spinel Raman and infrared spectra patterns were also analyzed according to the quasi-molecular description, using the internal modes for the FeO_4 tetrahedron.⁷³ So, in this case the structures was described as formed by two different sub-lattice groups: Fe^B/M atoms and $(\text{FeO}_4)^{5-}$ tetrahedron. Tables 2 and 3 summarize the FeO_4 group vibrations obtained by the correlation diagrams for cubic and tetragonal structures, respectively.

According to the FeO_4 symmetry, $\nu_1(A_1)$ and $\nu_3(F_2)$ are assigned to the Fe–O symmetric and asymmetric stretchings, respectively; while $\nu_2(E)$ and $\nu_1(F_2)$ vibrational modes are attributed to the symmetric and asymmetric Fe-O bendings. The $T(F_2)$ vibrational mode is assigned to the FeO_4 tetrahedron translation motion. Finally, the Raman and infrared modes for both cubic and tetragonal inverse spinels, disregarding the acoustic and silent modes, are shown in Table 4.

Table 1: Factor group analysis from CoFe_2O_4 (cubic) and CuFe_2O_4 (tetragonal)

Structure	Atoms	Sites	Site symmetry	Irreducible representations
Cubic (O_h^7)	Fe/Co	16d	D_{3d}	$A_{2u} \oplus E_u \oplus 2F_{1u} \oplus F_{2u}$
	Fe	8a	T_d	$F_{1u} \oplus F_{2g}$
	O	32e	C_{3v}	$A_{1g} \oplus A_{2u} \oplus E_g \oplus E_u \oplus F_{1g} \oplus 2F_{1u} \oplus 2F_{2g} \oplus F_{2u}$
			Total	$A_{1g} \oplus 2A_{2u} \oplus E_g \oplus 2E_u \oplus F_{1g} \oplus 5F_{1u} \oplus 3F_{2g} \oplus 2F_{2u}$
			Acoustic modes	F_{1u}
			IR modes	$4F_{1u}$
Tetragonal (D_{4h}^{19})	Fe/Cu	8d	C_{2h}	$A_{1u} \oplus 2A_{2u} \oplus B_{1u} \oplus 2B_{2u} \oplus 3E_u$
	Fe	4a	D_{2d}	$A_{2u} \oplus B_{1g} \oplus E_g \oplus E_u$
	O	16h	C_s^v	$2A_{1g} \oplus A_{1u} \oplus A_{2g} \oplus 2A_{2u} \oplus 2B_{1g} \oplus B_{1u} \oplus B_{2g} \oplus 2B_{2u} \oplus 3E_g \oplus 3E_u$
			Total	$2A_{1g} \oplus 2A_{1u} \oplus A_{2g} \oplus 5A_{2u} \oplus 3B_{1g} \oplus 2B_{1u} \oplus B_{2g} \oplus 4B_{2u} \oplus 4E_g \oplus 7E_u$
			Acoustic modes	$A_{2u} \oplus E_u$
			IR modes	$4A_{2u} \oplus 6E_u$
		Raman modes	$2A_{1g} \oplus 3B_{1g} \oplus B_{2g} \oplus 4E_g$	
		Silent modes	$2A_{1u} \oplus A_{2g} \oplus 2B_{1u} \oplus 4B_{2u}$	

Table 2: Correlation charts of the phonon symmetry for AFe_2O_4 in the (O_h^7) cubic structure.

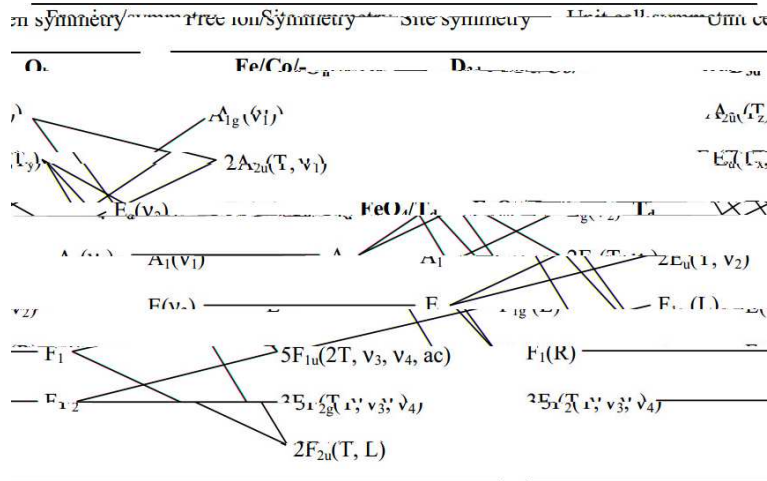


Table 3: Correlation charts of the phonon symmetry for AFe_2O_4 in the (D_{4h}^{19}) tetragonal phase.

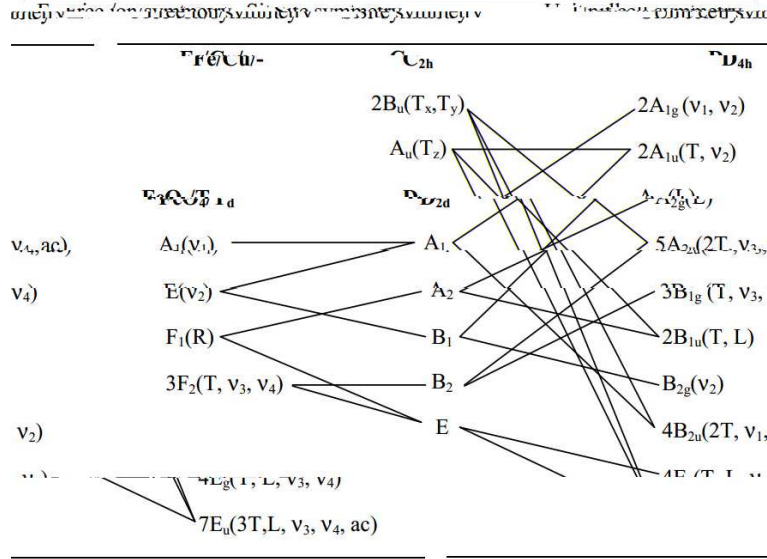


Table 4: Raman and Infrared modes corresponding to the cubic and tetragonal inverse spinels

Spinel structure	Activity	Assignments
$D_{4h}^{19}(\text{CuFe}_2\text{O}_4)$	Raman	$2T(B_{1g} \oplus E_g) + L(E_g) + v_1(A_{1g}) + 2v_2(A_{1g} \oplus B_{2g}) + 2v_3(B_{1g} \oplus E_g) + 2v_4(B_{1g} \oplus E_g)$
	IR	$5T(2A_{2u} \oplus 3E_u) + L(E_u) + 2v_3(A_{2u} \oplus E_u) + 2v_4(A_{2u} \oplus E_u)$
$O_h^7(\text{CoFe}_2\text{O}_4)$	Raman	$T(F_{2g}) \oplus v_1(A_{1g}) \oplus v_2(E_g) \oplus v_3(F_{2g}) \oplus v_4(F_{2g})$
	IR	$2T(2F_{1u}) \oplus v_3(F_{1u}) \oplus v_4(F_{1u})$

Results and Discussions

Structural properties

Figures 1 and 2 present the XRD patterns for the several $\text{Co}_{1-x}\text{Cu}_x\text{Fe}_2\text{O}_4$ spinel powders as a function of the annealing temperature. The results confirm the formation of the single phase spinel, as indicated by the JCPDS 00-034-0425 (tetragonal CuFe_2O_4) and JCPDS 00-022-1086 (cubic CoFe_2O_4) patterns, excepted for those annealed at 700 and 800 °C Cu-based pure spinels that contain $\alpha\text{-Fe}_2\text{O}_3$ rhombohedral (JCPDS 00-013-0534). It is important to point out that $\alpha\text{-Fe}_2\text{O}_3$ is often found as a secondary phase in spinel synthesis, as previously reported by Sun et al.⁶² and Mathew et al.⁷⁴ In addition, for the cobalt substituted ferrites, it can be noticed that even minor Co^{2+} inclusions induce a cubic lattice. The full-width at half maximum (FWHM) (monitoring the peak (400)) in CoFe_2O_4 decreases with the increase of the annealing temperature, as shown in Figure 3, showing that the average crystallite size is becoming larger, while an inverse behavior is observed in CuFe_2O_4 (monitoring the peak (211)). Besides, for $\text{Co}_{0.25}\text{Cu}_{0.75}\text{Fe}_2\text{O}_4$ samples, the FWHM hardly changes, except when synthesized at 900 °C and above. This behavior could be associated to minor lattice distortion imposed by the spatial competition between octahedral and tetrahedral sites. Such fact is confirmed by Figure 4, since Co-substituted ferrites present bigger average crystallite sizes, as compared to the CuFe_2O_4 structures. Furthermore, the average crystallite size tends to enlarge with the annealing (26 up to 54 nm). Specifically, CuFe_2O_4 crystallites show mean size between 32 and 35 nm, much lower than the value proposed by Sun et al.,⁶² that estimated the range in between 75 - 110 nm for the ferrites. In opposition, CoFe_2O_4 crystallite sizes were in the range 28 - 37 nm, being also smaller than those reported by Gaikwad *et al.*,⁷⁵ i.e., 60 - 80 nm, but bigger than the one obtained by Valdés-Solís *et al.*,⁷⁶ that was 20 nm.

Vibrational properties

Figure 5 shows the Raman spectra obtained for CoFe_2O_4 and CuFe_2O_4 pure annealed spinels. CuFe_2O_4 spinel, synthesized at 700 and 800 °C (Figure 5b), in fact corresponds to the $\alpha\text{-Fe}_2\text{O}_3$ as

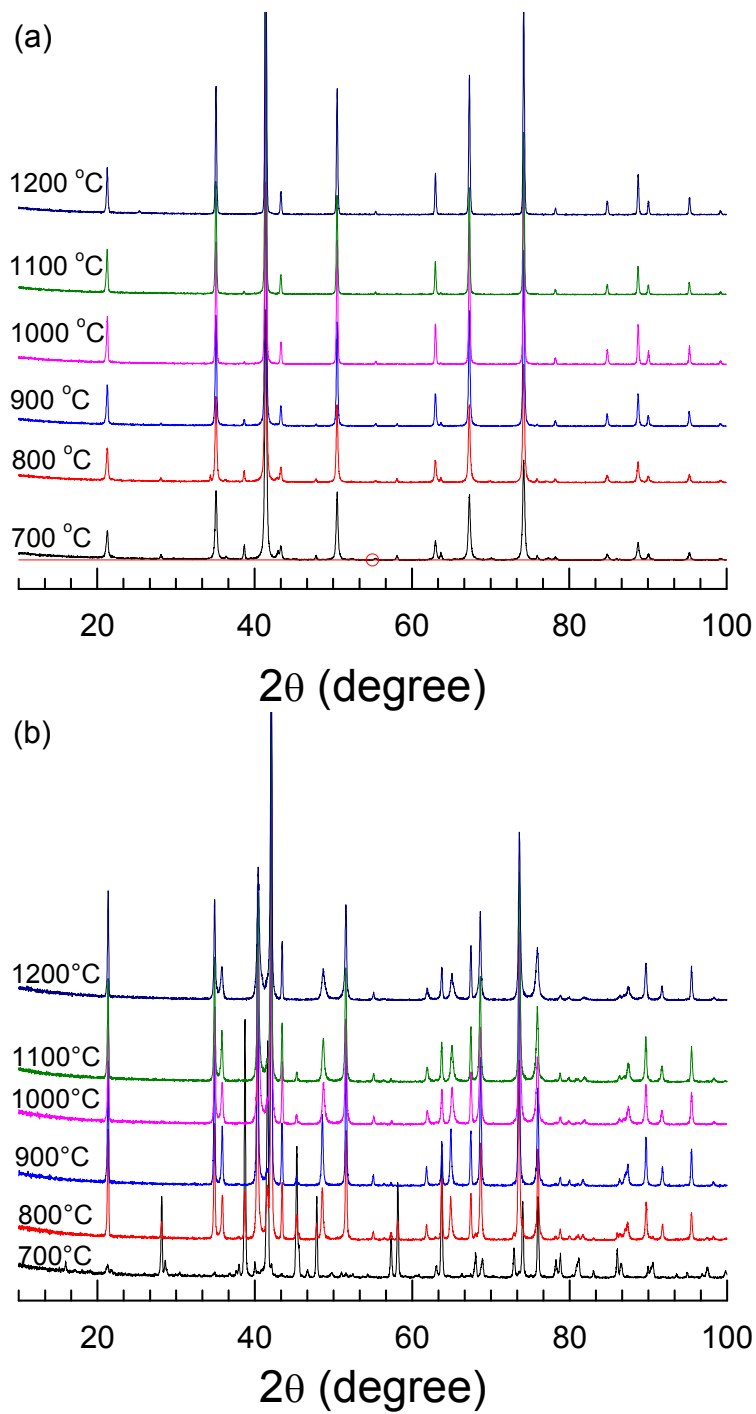


Figure 1: XRD patterns as function of the annealing temperature for (a) CoFe_2O_4 and (b) CuFe_2O_4 spinels.

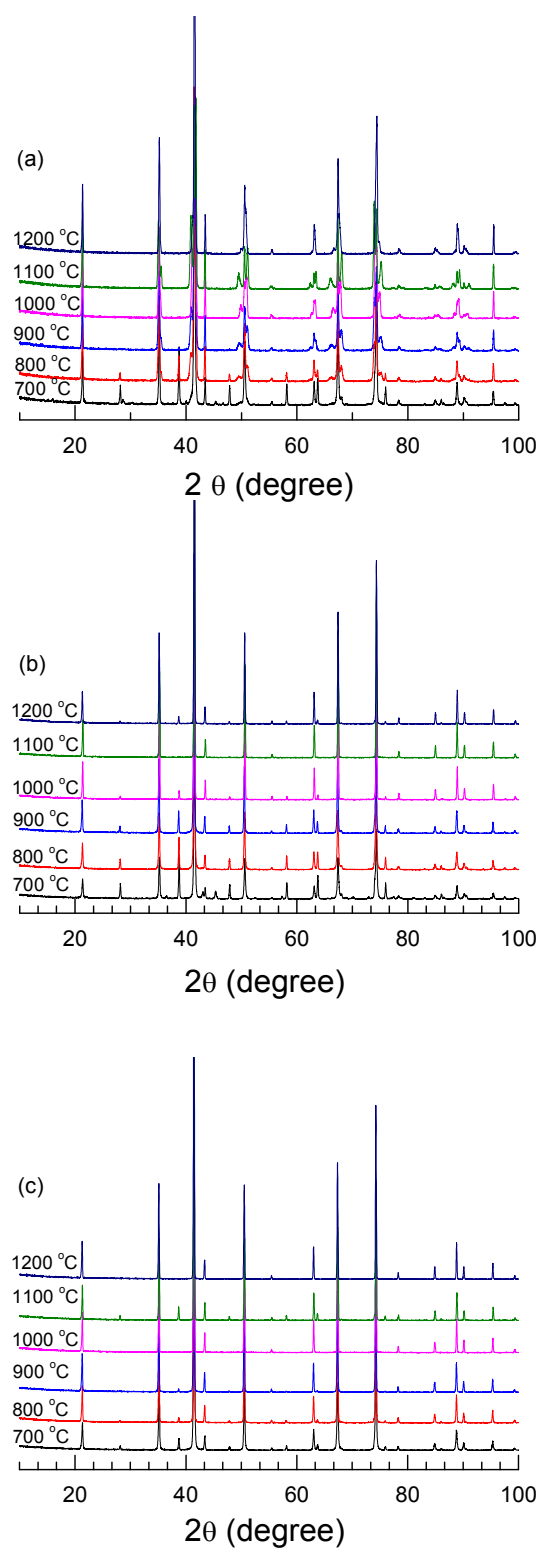


Figure 2: XRD patterns as function of the annealing temperature for (a) $\text{Co}_{0.25}\text{Cu}_{0.75}\text{Fe}_2\text{O}_4$. (b) $\text{Co}_{0.50}\text{Cu}_{0.50}\text{Fe}_2\text{O}_4$ and (c) $\text{Co}_{0.75}\text{Cu}_{0.25}\text{Fe}_2\text{O}_4$ spinels.

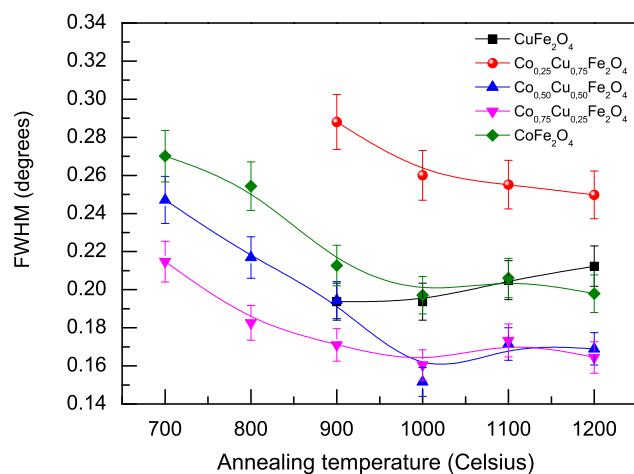


Figure 3: FWHM as function of the annealing temperature for the $\text{Co}_{1-x}\text{Cu}_x\text{Fe}_2\text{O}_4$ ($x = 1.00, 0.75, 0.50, 0.25, 0.00$) spinels. The lines are guides for the eyes.

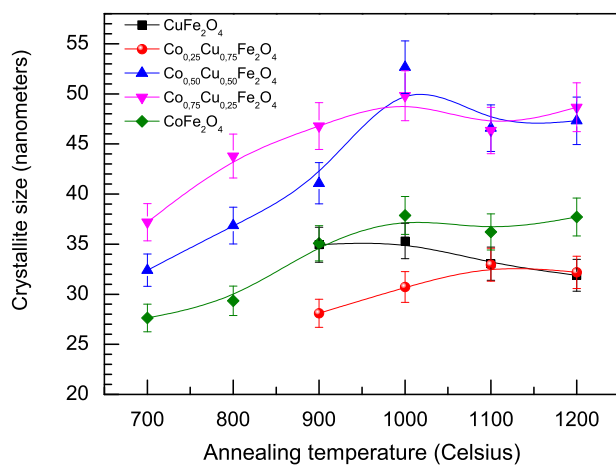


Figure 4: Crystallite size as function of the ternary thermal treatment for the $\text{Co}_{1-x}\text{Cu}_x\text{Fe}_2\text{O}_4$ ($x = 1.00, 0.75, 0.50, 0.25, 0.00$) spinels. The lines are guides for the eyes.

confirmed by their Raman spectra and supported by the XRD results.⁷⁷ Nonetheless, for higher annealing temperatures (900 - 1200°C), eight characteristic vibrational modes (Table 5) attributed to the monophasic CuFe_2O_4 structure are depicted from the spectra and such result agrees with group theory prediction. CoFe_2O_4 sample spectra (Figure 5a) exhibit only five broad bands around 180, 315, 480, 640 and 680 cm^{-1} , all of them assigned to the cubic inverse-spinel ferrites^{73,77-88}. In this structure the modes around 180 and 300 cm^{-1} are assigned to the $T(F_{2g})$ and $\nu_2(E_g)$ modes, respectively. Also, the modes $\nu_4(F_{2g})$, $\nu_3(F_{2g})$ and $\nu_1(A_{1g})$ are observed at 460, 590 and 680 cm^{-1} , respectively.

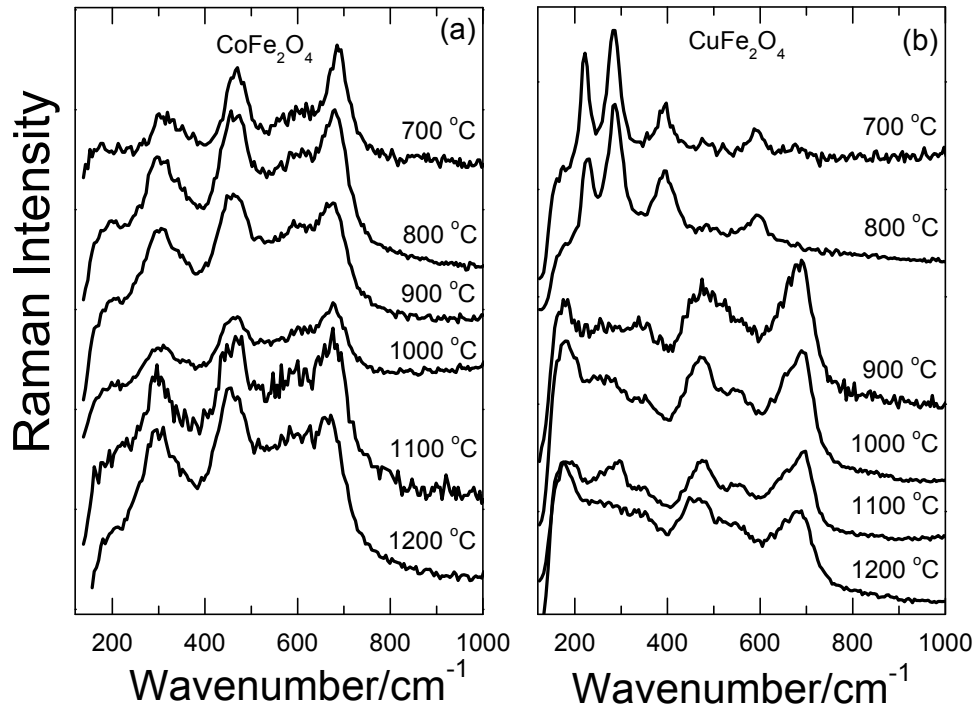


Figure 5: Room temperature Raman spectra for (a) CoFe_2O_4 and (b) CuFe_2O_4 investigated spinels.

Table 5 summarizes the symmetry assignments to the observed Raman-active modes of the several spinel samples investigated in this work. The wavenumber of the peaks indicated were found by fitting Raman spectra with Lorentzian functions. In general, the phonon spectral positions are essentially independent of the annealing temperature for all compounds.

Figure 6 shows the Raman spectra obtained from all mixed spinels ($x = 0.75, 0.5$ and 0.25).

Table 5: Wavenumbers (in cm^{-1}) and Raman modes assignments for $\text{Co}_{1-x}\text{Cu}_x\text{Fe}_2\text{O}_4$ ($x = 1.00, 0.75, 0.50, 0.25, 0.00$) spinels.

Compound	modes	Annealing temperature ($^{\circ}\text{C}$)						Assignment
		700	800	900	1000	1100	1200	
CoFe₂O₄	1	171	170	169	169	179	188	T(F_{2g})
	2	315	300	295	294	296	297	$\nu_2(\text{E}_g)$
	3	468	462	459	460	458	456	$\nu_4(\text{F}_{2g})$
	4	599	595	592	593	596	588	$\nu_3(\text{F}_{2g})$
	5	687	682	678	679	680	672	$\nu_1(\text{A}_{1g})$
Co_{0.75}Cu_{0.25}Fe₂O₄	1	192	183	193	189	188	192	T
	2	300	308	298	303	309	303	ν_2
	3	355	355	–	359	–	363	ν_4
	4	464	469	466	468	468	468	ν_4
	5	552	–	563	569	575	570	ν_3
	6	608	602	619	626	–	–	ν_3
	7	–	659	–	–	657	641	ν_3
	8	681	693	688	690	692	692	ν_1
Co_{0.50}Cu_{0.50}Fe₂O₄	1	196	189	203	180	188	187	T
	2	–	–	–	239	239	245	T/L
	3	303	300	312	309	311	313	ν_2
	4	–	–	–	379	374	368	ν_4
	5	467	471	469	472	470	473	ν_4
	6	610	604	605	576	573	592	ν_3
	7	–	–	–	678	662	672	ν_3
	8	688	689	687	702	696	698	ν_1
Co_{0.25}Cu_{0.75}Fe₂O₄	1	171	170	170	172	174	177	T
	2	197	194	194	198	200	214	T/L
	3	238	230	239	245	268	266	ν_2
	4	320	313	322	321	346	331	ν_4
	5	482	468	466	460	475	463	ν_4
	6	586	582	597	588	577	587	ν_3
	7	685	651	682	673	667	659	ν_3
	8	712	693	711	702	701	694	ν_1
CuFe₂O₄	1	–	–	177	171	177	168	T
	2	–	–	250	244	245	211	T/L
	3	–	–	–	–	294	271	ν_2
	4	–	–	343	348	348	346	ν_4
	5	–	–	467	469	474	462	ν_4
	6	–	–	532	554	554	549	ν_3
	7	–	–	663	658	655	656	ν_3
	8	–	–	694	696	696	692	ν_1

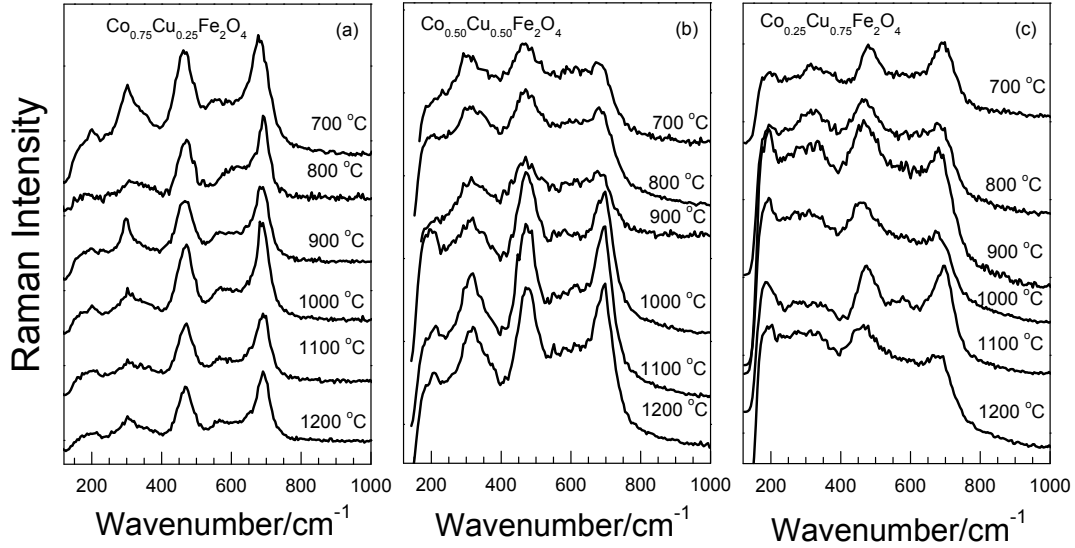


Figure 6: Room temperature Raman spectra for (a) $\text{Co}_{0.75}\text{Cu}_{0.25}\text{Fe}_2\text{O}_4$, (b) $\text{Co}_{0.50}\text{Cu}_{0.50}\text{Fe}_2\text{O}_4$ and (c) $\text{Co}_{0.25}\text{Cu}_{0.75}\text{Fe}_2\text{O}_4$ spinels.

Although the XRD patterns suggest that all Cobalt-doped samples' structures are cubic, the Raman spectra reveals that $\text{Co}_{0.25}\text{Cu}_{0.25}\text{Fe}_2\text{O}_4$, $\text{Co}_{0.50}\text{Cu}_{0.50}\text{Fe}_2\text{O}_4$ and $\text{Co}_{0.75}\text{Cu}_{0.25}\text{Fe}_2\text{O}_4$ locally assume tetragonal structures. Such discrepancy is explained localized nature of Raman spectroscopy in contrast to the averaged one of XRD. Besides, no significant wavenumber mode dependence was observed with Cobalt substitution.

Figure 7 shows that the room temperature mid IR spectra observed for CuFe_2O_4 and CoFe_2O_4 spinels are in good agreement with those reported by previous works.^{63,89-96} According to Selvan et al.⁶³ and Dey et al.⁹⁷ CuFe_2O_4 powders have two characteristic vibrational modes about 600 and 400 cm^{-1} , which are attributed to the tetrahedral and octahedral M^{2+} cations, respectively. In this work, such stretching modes are detected around 474 - 397 cm^{-1} [$\nu(\text{Fe-O})_B$], 531- 559 cm^{-1} [$\nu(\text{Fe-O})_A$] and 605 - 672 cm^{-1} [$\nu(\text{Cu-O})_A$], in which both Fe-O modes are assigned to the F_{1u} symmetry (Figure 7). The higher wavenumber values for the A-site cations results from the shortening $\text{M}^{2+}\text{-O}^{2-}$ bond length at such symmetries.⁹⁸

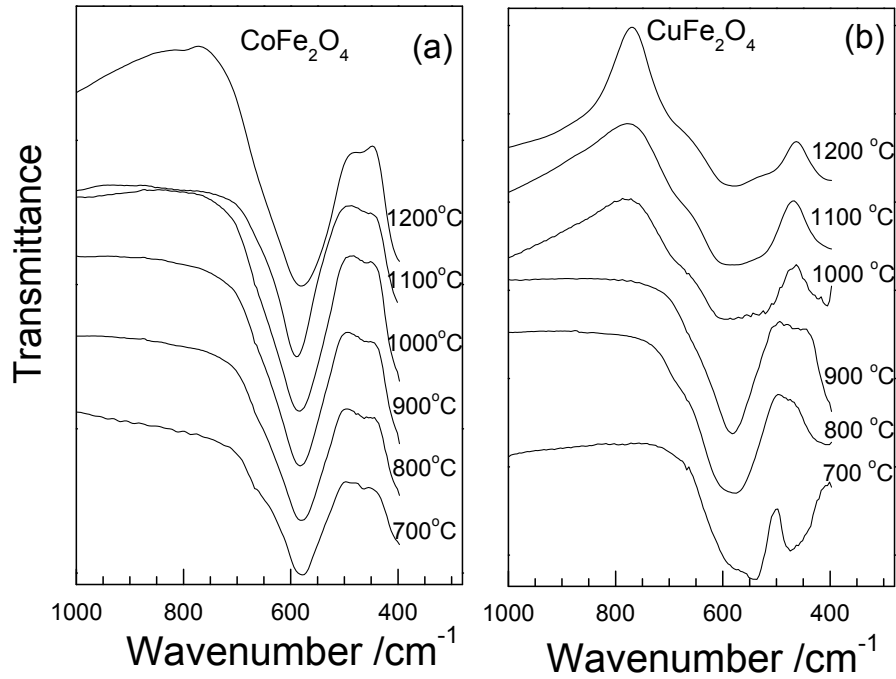


Figure 7: Room temperature IR spectra of (a) CoFe_2O_4 and (b) CuFe_2O_4 investigated spinels.

Once again, the $\alpha\text{-Fe}_2\text{O}_3$ phase is depicted from the spectra of CuFe_2O_4 samples annealed at 700 °C and 900 °C, as indicated by the strong absorption band at 475 cm^{-1} [$\nu(\text{Fe-O})$].⁹⁹ Finally, the CuFe_2O_4 samples obtained at 1000, 1100 and 1200 °C present a significant tetragonal distortion (Jahn-Teller distortion), corroborating to the Raman and XRD data.

Considering the CoFe_2O_4 sample, similar vibrational modes are observed around 399 - 400 [$\nu(\text{Fe-O})_B$], 464 - 541 [$\nu(\text{Fe-O})_A$] and 576 - 583 [$\nu(\text{Co-O})_A$] (Figure 7a). The displacement of the $(\text{Co-O})_A$ modes to lower wavenumbers, as compared to the $(\text{Cu-O})_A$ one, results from the smaller cobalt ionic radius, generating a larger vibrational energy.^{100–102}

The Co-substituted CuFe_2O_4 IR spectra (Figure 8) show a continuous band narrowing as function of cobalt contents into the lattice. Nevertheless, the same tetrahedral and octahedral vibrational modes are assigned.

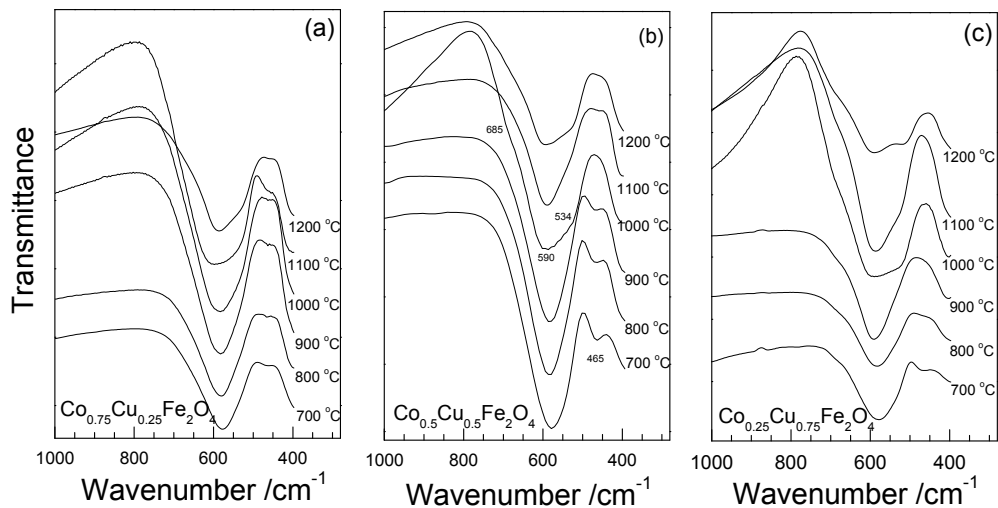


Figure 8: Room temperature IR spectra of (a) $\text{Co}_{0.75}\text{Cu}_{0.25}\text{Fe}_2\text{O}_4$, (b) $\text{Co}_{0.50}\text{Cu}_{0.50}\text{Fe}_2\text{O}_4$ and (c) $\text{Co}_{0.25}\text{Cu}_{0.75}\text{Fe}_2\text{O}_4$ spinels.

Conclusions

In this work we have synthesized nanometric $\text{Co}_{1-x}\text{Cu}_x\text{Fe}_2\text{O}_4$ spinels using a polymeric precursors method precursors. The crystalline structures were investigated by X-ray powder diffraction, which confirms that the pure CoFe_2O_4 and CuFe_2O_4 samples have cubic and tetragonal inverted spinel structures, respectively. The crystallite sizes of the mixed samples are bigger than those of the pure samples. The synthesized samples were investigated by Raman and infrared spectroscopies. This analysis showed that there is a tetragonal local distortion into the mixed sample. A complete mode assignment for all the samples was performed based on the internal vibrations of the FeO_4 molecular group.

Acknowledgement

The authors are grateful to the Brazilian funding agencies CAPES, CNPq, and FAPEMA.

References

- (1) Cheong, S.-W.; Mostovoy, M. *NATURE MATERIALS* **2007**, *6*, 13–20.
- (2) Chiba, D.; Sawicki, M.; Nishitani, Y.; Nakatani, Y.; Matsukura, F.; Ohno, H. *NATURE* **2008**, *455*, 515–518.
- (3) Eerenstein, W.; Wiora, M.; Prieto, J. L.; Scott, J. F.; Mathur, N. D. *NATURE MATERIALS* **2007**, *6*, 348–351.
- (4) Ramesh, R.; Spaldin, N. A. *NATURE MATERIALS* **2007**, *6*, 21–29.
- (5) Scott, J. F. *Nature Materials* **2007**, *6*, 256–257.
- (6) Bea, H.; Paruch, P. *NATURE MATERIALS* **2009**, *8*, 168–U14.
- (7) Chu, Y.-H. et al. *NATURE MATERIALS* **2008**, *7*, 478–482.
- (8) Seidel, J. et al. *NATURE MATERIALS* **2009**, *8*, 229–234.
- (9) Yang, C. H. et al. *NATURE MATERIALS* **2009**, *8*, 485–493.
- (10) Zhao, T.; Scholl, A.; Zavaliche, F.; Lee, K.; Barry, M.; Doran, A.; Cruz, M. P.; Chu, Y. H.; Ederer, C.; Spaldin, N. A.; Das, R. R.; Kim, D. M.; Baek, S. H.; Eom, C. B.; Ramesh, R. *NATURE MATERIALS* **2006**, *5*, 823–829.
- (11) Aguilar, R. V.; Mostovoy, M.; Sushkov, A. B.; Zhang, C. L.; Choi, Y. J.; Cheong, S.-W.; Drew, H. D. *PHYSICAL REVIEW LETTERS* **2009**, *102*, 047203.
- (12) Bea, H.; Bibes, M.; Ott, F.; Dupe, B.; Zhu, X. H.; Petit, S.; Fusil, S.; Deranlot, C.; Bouzehouane, K.; Barthelemy, A. *PHYSICAL REVIEW LETTERS* **2008**, *100*, 017204.
- (13) Kornev, I. A.; Lisenkov, S.; Haumont, R.; Dkhil, B.; Bellaiche, L. *PHYSICAL REVIEW LETTERS* **2007**, *99*, 227602.

- (14) Wang, J.; Neaton, J.; Zheng, H.; Nagarajan, V.; Ogale, S.; Liu, B.; Viehland, D.; Vaithyanathan, V.; Schlom, D.; Waghmare, U.; Spaldin, N.; Rabe, K.; Wuttig, M.; Ramesh, R. *SCIENCE* **2003**, *299*, 1719–1722.
- (15) Kimura, T.; Goto, T.; Shintani, H.; Ishizaka, K.; Arima, T.; Tokura, Y. *NATURE* **2003**, *426*, 55–58.
- (16) Lee, S.; Pirogov, A.; Kang, M.; Jang, K.-H.; Yonemura, M.; Kamiyama, T.; Cheong, S. W.; Gozzo, F.; Shin, N.; Kimura, H.; Noda, Y.; Park, J. G. *NATURE* **2008**, *451*, 805–U4.
- (17) Pimenov, A.; Shuvaev, A.; Loidl, A.; Schrettle, F.; Mukhin, A. A.; Travkin, V. D.; Ivanov, V. Y.; Balbashov, A. M. *PHYSICAL REVIEW LETTERS* **2009**, *102*, 107203.
- (18) Bodenthin, Y.; Staub, U.; Garcia-Fernandez, M.; Janoschek, M.; Schlappa, J.; Golovenchits, E. I.; Sanina, V. A.; Lushnikov, S. G. *PHYSICAL REVIEW LETTERS* **2008**, *100*, 027201.
- (19) Harris, A. B.; Aharony, A.; Entin-Wohlman, O. *PHYSICAL REVIEW LETTERS* **2008**, *100*, 217202.
- (20) Okamoto, J.; Huang, D. J.; Mou, C. Y.; Chao, K. S.; Lin, H. J.; Park, S.; Cheong, S.-W.; Chen, C. T. *PHYSICAL REVIEW LETTERS* **2007**, *98*, 157202.
- (21) Sushkov, A. B.; Aguilar, R. V.; Cheong, S.-W.; Drew, H. D. *PHYSICAL REVIEW LETTERS* **2007**, *98*, 027202.
- (22) Wang, F.; Vishwanath, A. *PHYSICAL REVIEW LETTERS* **2008**, *100*, 077201.
- (23) Ye, F.; Fernandez-Baca, J. A.; Fishman, R. S.; Ren, Y.; Kang, H. J.; Qiu, Y.; Kimura, T. *PHYSICAL REVIEW LETTERS* **2007**, *99*, 157201.
- (24) Choi, Y. J.; Okamoto, J.; Huang, D. J.; Chao, K. S.; Lin, H. J.; Chen, C. T.; van Veenendaal, M.; Kaplan, T. A.; Cheong, S.-W. *PHYSICAL REVIEW LETTERS* **2009**, *102*, 067601.

- (25) Kimura, T.; Lawes, G.; Ramirez, A. *PHYSICAL REVIEW LETTERS* **2005**, *94*, 137201.
- (26) Li, L.; Lin, Y. Q.; Chen, X. M. *Journal of Applied Physics* **2007**, *102*.
- (27) Wang, Z. G.; Viswan, R.; Hu, B. L.; Harris, V. G.; Li, J. F.; Viehland, D. *Physica Status Solidi-Rapid Research Letters* **2012**, *6*, 92–94.
- (28) Yan, L. H.; Liang, W. Z.; Liu, S. H.; Huang, W.; Lin, Y. *INTEGRATED FERROELECTRICS* **2011**, *131*, 82–88.
- (29) Wang, J.-N.; Li, W.-L.; Li, X.-L.; Fei, W. D. *POWDER DIFFRACTION* **2010**, *25*, S45–S47, 10th Chinese National Conference on X-Ray Diffraction/ICDD Workshop, Shanghai, PEOPLES R CHINA, OCT 12-15, 2009.
- (30) Chen, W.; Shannigrahi, S.; Chen, X. F.; Wang, Z. H.; Zhu, W.; Tan, O. K. *SOLID STATE COMMUNICATIONS* **2010**, *150*, 271–274.
- (31) Zhang, L.; Zhai, J.; Mo, W.; Yao, X. *FERROELECTRICS* **2010**, *406*, 213–220.
- (32) Zhang, J. X.; Dai, J. Y.; Lu, W.; Chan, H. L. W. *JOURNAL OF MATERIALS SCIENCE* **2009**, *44*, 5143–5148.
- (33) Yan, L.; Xing, Z.; Wang, Z.; Wang, T.; Lei, G.; Li, J.; Viehland, D. *APPLIED PHYSICS LETTERS* **2009**, *94*, 192902.
- (34) Wu, X.; Cai, W.; Kan, Y.; Yang, P.; Liu, Y.; Bo, H.; Lu, X.; Zhu, J. *FERROELECTRICS* **2009**, *380*, 48–55, 6th Asian Meeting on Ferroelectrics, Taipei, TAIWAN, AUG 02-06, 2008.
- (35) Pang, L.-H.; Ji, W.-J.; Zhang, Y.; Wang, L.; Zhang, S.-T.; Luo, Z.-L.; Chen, Y.-F. *JOURNAL OF PHYSICS D-APPLIED PHYSICS* **2009**, *42*, 045304.
- (36) Chen, W.; Wang, Z. H.; Zhu, W.; Tan, O. K. *JOURNAL OF PHYSICS D-APPLIED PHYSICS* **2009**, *42*, 075421.

- (37) Dix, N.; Skumryev, V.; Laukhin, V.; Fabrega, L.; Sanchez, F.; Fontcuberta, J. *MATERIALS SCIENCE AND ENGINEERING B-SOLID STATE MATERIALS FOR ADVANCED TECHNOLOGY* **2007**, *144*, 127–131, Symposium on Nanoscale Tailoring of Defect Structures for Optimized Functional and Multifunctional Oxide Films held at the EMRS 2007, Strasbourg, FRANCE, 2007.
- (38) Thang, P. D.; Pham, M. T. N.; Rijnders, G.; Blank, D. H. A.; Duc, N. H.; Klaasse, J. C. P.; Bruck, E. *JOURNAL OF THE KOREAN PHYSICAL SOCIETY* **2008**, *52*, 1406–1409, 1st International Workshop on Functional Materials/3rd International Workshop on Nanophysics and Nanotechnology, Halong City, VIETNAM, DEC 06-09, 2006.
- (39) Ederer, C.; Spaldin, N. *PHYSICAL REVIEW LETTERS* **2005**, *95*, 257601.
- (40) Tokunaga, Y.; Furukawa, N.; Sakai, H.; Taguchi, Y.; Arima, T.-h.; Tokura, Y. *NATURE MATERIALS* **2009**, *8*, 558–562.
- (41) Sun, J. R.; Wang, Z. G.; Wang, Y. Y.; Zhu, Y. B.; Shen, T. L.; Pang, L. L.; Wei, K. F.; Li, F. S. *Materials Science and Engineering B-Advanced Functional Solid-State Materials* **2012**, *177*, 269–273.
- (42) Tang, Y.; Wang, X. W.; Zhang, Q. H.; Li, Y. G.; Wang, H. Z. *Progress in Natural Science-Materials International* **2012**, *22*, 53–58.
- (43) Pui, A.; Gherca, D.; Carja, G. *Digest Journal of Nanomaterials and Biostructures* **2011**, *6*, 1783–1791.
- (44) Girgis, E.; Wahsh, M. M. S.; Othman, A. G. M.; Bandhu, L.; Rao, K. V. *NANOSCALE RESEARCH LETTERS* **2011**, *6*, 460.
- (45) Fei, C. L.; Zhang, Y.; Yang, Z.; Liu, Y.; Xiong, R.; Shi, J.; Ruan, X. F. *Journal of Magnetism and Magnetic Materials* **2011**, *323*, 1811–1816.

- (46) Naseri, M. G.; Saion, E. B.; Hashim, M.; Shaari, A. H.; Ahangar, H. A. *Solid State Communications* **2011**, *151*, 1031–1035.
- (47) El-Okr, M. M.; Salem, M. A.; Salim, M. S.; El-Okr, R. M.; Ashoush, M.; Talaat, H. M. *Journal of Magnetism and Magnetic Materials* **2011**, *323*, 920–926.
- (48) Gatelyte, A.; Jasaitis, D.; Beganskiene, A.; Kareiva, A. *Materials Science-Medziagotyra* **2011**, *17*, 302–307.
- (49) Yu, B. Y.; Kwak, S. Y. *Dalton Transactions* **2011**, *40*, 9989–9998.
- (50) Gatelyte, A.; Jasaitis, D.; Beganskiene, A.; Kareiva, A. *Materials Science-Medziagotyra* **2011**, *17*, 302–307.
- (51) Shen, L. M.; Bao, N. Z.; Prevelige, P. E.; Gupta, A. *Journal of the American Chemical Society* **2010**, *132*, 17354–17357.
- (52) Zhang, Y.; Yang, Z.; Yin, D.; Liu, Y.; Fei, C. L.; Xiong, R.; Shi, J.; Yan, G. L. *Journal of Magnetism and Magnetic Materials* **2010**, *322*, 3470–3475.
- (53) Ajroudi, L.; Villain, S.; Madigou, V.; Mliki, N.; Leroux, C. *Journal of Crystal Growth* **2010**, *312*, 2465–2471.
- (54) Veverka, M.; Veverka, P.; Jirak, Z.; Kaman, O.; Knizek, K.; Marysko, M.; Pollert, E.; Záveta, K. *Journal of Magnetism and Magnetic Materials* **2010**, *322*, 2386–2389.
- (55) Sertkol, M.; Koseoglu, Y.; Baykal, A.; Kavas, H.; Toprak, M. S. *Journal of Magnetism and Magnetic Materials* **2010**, *322*, 866–871.
- (56) Shahane, G. S.; Kumar, A.; Arora, M.; Pant, R. P.; Lal, K. *Journal of Magnetism and Magnetic Materials* **2010**, *322*, 1015–1019.
- (57) Hou, C. Y.; Yu, H.; Zhang, Q. H.; Li, Y. G.; Wang, H. Z. *Journal of Alloys and Compounds* **2010**, *491*, 431–435.

- (58) Shen, X. Q.; Zhou, Z.; Song, F. Z.; Meng, X. F. *Journal of Sol-Gel Science and Technology* **2010**, *53*, 405–411.
- (59) Manova, E.; Paneva, D.; Kunev, B.; Estournes, C.; Riviere, E.; Tenchev, K.; Leautic, A.; Mitov, I. *JOURNAL OF ALLOYS AND COMPOUNDS* **2009**, *485*, 356–361.
- (60) Gozuak, F.; Koseoglu, Y.; Baykal, A.; Kavasa, H. *Journal of Magnetism and Magnetic Materials* **2009**, *321*, 2170–2177.
- (61) Maaz, K.; Karim, S.; Mumtaz, A.; Hasanain, S. K.; Liu, J.; Duan, J. L. *Journal of Magnetism and Magnetic Materials* **2009**, *321*, 1838–1842.
- (62) Sun, Z.; Liu, L.; zeng Jia, D.; Pan, W. *Sensors and Actuators B: Chemical* **2007**, *125*, 144 – 148.
- (63) Selvan, R.; Augustin, C.; Berchmans, L.; Saraswathi, R. *MATERIALS RESEARCH BULLETIN* **2003**, *38*, 41–54.
- (64) Sawatzky, G. A.; Vanderwo, F.; Morrish, A. H. *PHYSICAL REVIEW* **1969**, *183*, 383–386.
- (65) Nedkov, I.; Vandenberghe, R. E.; Marinova, T.; Thailhades, P.; Merodiiska, T.; Avramova, I. *APPLIED SURFACE SCIENCE* **2006**, *253*, 2589–2596.
- (66) Yokoyama, M.; Nakamura, A.; Sato, T.; Haneda, K. *JOURNAL OF THE MAGNETICS SOCIETY OF JAPAN* **1998**, *22*, 243–245.
- (67) Kester, E.; Gillot, B.; Villette, P., C. Tailhades; Rousset, A. *THERMOCHIMICA ACTA* **1997**, *297*, 71–78.
- (68) Jiang, J. Z.; Goya, G. F.; Rechenberg, H. R. *JOURNAL OF PHYSICS-CONDENSED MATTER* **1999**, *11*, 46063–4078.
- (69) Hamdeh, H.; Ho, J.; Oliver, S.; Willey, R.; Oliver, G.; Busca, G. *JOURNAL OF APPLIED PHYSICS* **1997**, *81*, 1851–1857.

- (70) Sreekumar, K.; Mathew, T.; Devassy, B.; Rajgopal, R.; Vetrivel, R.; Rao, B. *APPLIED CATALYSIS A-GENERAL* **2001**, *205*, 11–18.
- (71) Tao, S.; Gao, F.; Liu, X.; Sorensen, O. T. *Materials Science and Engineering: B* **2000**, *77*, 172 – 176.
- (72) Rousseau, D. L.; Bauman, R. P.; Porto, S. P. S. *JOURNAL OF RAMAN SPECTROSCOPY* **1981**, *10*, 253–290.
- (73) VERBLE, J. *PHYSICAL REVIEW B* **1974**, *9*, 5236–5248.
- (74) Mathew, T.; Shylesh, S.; Devassy, B.; Vijayaraj, M.; Satyanarayana, C.; Rao, B.; Gopinath, C. *APPLIED CATALYSIS A-GENERAL* **2004**, *273*, 35–45.
- (75) Gaikwad, R. S.; Chae, S.-Y.; Mane, R. S.; Han, S.-H.; Joo, O.-S. *International Journal of Electrochemistry* **2011**, *2011*, 729141.
- (76) Valdes-Solis, T.; Tartaj, P.; Marban, G.; Fuertes, A. B. *NANOTECHNOLOGY* **2007**, *18*, 145603.
- (77) Shebanova, O.; Lazor, P. *JOURNAL OF SOLID STATE CHEMISTRY* **2003**, *174*, 424–430.
- (78) Gupta, R.; Sood, A.; Metcalf, P.; Honig, J. *PHYSICAL REVIEW B* **2002**, *65*, 104430.
- (79) Gasparov, L.; Tanner, D.; Romero, D.; Berger, H.; Margaritondo, G.; Forro, L. *PHYSICAL REVIEW B* **2000**, *62*, 7939–7944.
- (80) Li, J.; Huan, A.; Wang, L.; Du, Y.; Feng, D. *PHYSICAL REVIEW B* **2000**, *61*, 6876–6878.
- (81) Bersani, D.; Lottici, P.; Montenero, A. *JOURNAL OF RAMAN SPECTROSCOPY* **1999**, *30*, 355–360.
- (82) deFaria, D.; Silva, S.; deOliveira, M. *JOURNAL OF RAMAN SPECTROSCOPY* **1997**, *28*, 873–878.

- (83) THIERRY, D.; PERSSON, D.; LEYGRAF, C.; BOUCHERIT, N.; HUGOTLEGOFF, A. *CORROSION SCIENCE* **1991**, 32, 273–284.
- (84) BOUCHERIT, N.; GOFF, A.; JOIRET, S. *CORROSION SCIENCE* **1991**, 32, 497–507.
- (85) DUNNWALD, J.; OTTO, A. *CORROSION SCIENCE* **1989**, 29, 1167–1176.
- (86) GRAVES, P.; JOHNSTON, C.; CAMPANIELLO, J. *MATERIALS RESEARCH BULLETIN* **1988**, 23, 1651–1660.
- (87) DEGIORGI, L.; BLATTERMORKE, I.; WACHTER, P. *PHYSICAL REVIEW B* **1987**, 35, 5421–5424.
- (88) OHTSUKA, T.; KUBO, K.; SATO, N. *CORROSION* **1986**, 42, 476–481.
- (89) Hashim, M.; Alimuddin,; Kumar, S.; Koo, B. H.; Shirsath, S. E.; Mohammed, E. M.; Shah, J.; Kotnala, R. K.; Choi, H. K.; Chung, H.; Kumar, R. *JOURNAL OF ALLOYS AND COMPOUNDS* **2012**, 518, 11–18.
- (90) Eshraghi, M.; Kameli, P. *CURRENT APPLIED PHYSICS* **2011**, 11, 476–481.
- (91) Cedeno-Mattei, Y.; Perales-Perez, O. *MICROELECTRONICS JOURNAL* **2009**, 40, 673–676, Conference on European Nano Systems, Paris, FRANCE, DEC 03-04, 2007.
- (92) Zhao, L.; Zhang, H.; Xing, Y.; Song, S.; Yu, S.; Shi, W.; Guo, X.; Yang, J.; Lei, Y.; Cao, F. *JOURNAL OF SOLID STATE CHEMISTRY* **2008**, 181, 245–252.
- (93) Gillot, B.; Nivoix, V.; Kester, E.; Nusillard, O.; Villette, C.; Tailhades, P.; Rousset, A. *MATERIALS CHEMISTRY AND PHYSICS* **1997**, 48, 111–118.
- (94) Gillot, B.; Buguet, S.; Kester, E. *JOURNAL OF MATERIALS CHEMISTRY* **1997**, 7, 2513–2517.
- (95) Gillot, B.; Laarj, M.; Kacim, S. *JOURNAL OF MATERIALS CHEMISTRY* **1997**, 7, 827–831.

- (96) WALDRON, R. *PHYSICAL REVIEW* **1955**, *99*, 1727–1735.
- (97) Dey, S.; Ghose, J. *MATERIALS RESEARCH BULLETIN* **2003**, *38*, 1653–1660.
- (98) Costa, A. F.; Pimentel, P. M.; Melo, D. M. A.; Melo, M. A. F.; Aquino, F. M. *Cerâmica* **2011**, *57*, 352 – 355.
- (99) Gotic, M.; Jurkin, T.; Music, S. *COLLOID AND POLYMER SCIENCE* **2007**, *285*, 793–800.
- (100) Popmintchev, T.; Chen, M.-C.; Bahabad, A.; Gerrity, M.; Sidorenko, P.; Cohen, O.; Christov, I. P.; Murnane, M. M.; Kapteyn, H. C. *PROCEEDINGS OF THE NATIONAL ACADEMY OF SCIENCES OF THE UNITED STATES OF AMERICA* **2009**, *106*, 10516–10521.
- (101) Singhal, S.; Bhukal, S.; Singh, J.; Chandra, K.; Bansal, S. *Journal of Nanotechnology* **2011**, 930243.
- (102) Zhang, Y.; Wen, D. *Journal of the American Ceramic Society* **2012**, cited By (since 1996) 0; Article in Press.

Raman Intensity

